Received 31 May 2024; accepted 15 June 2024. Date of publication 19 June 2024; date of current version 26 July 2024.
The review of this article was arranged by Editor P.-W. Li.

Digital Object Identifier 10.1109/JEDS.2024.3416516

HfO_2 Thin Films by Chemical Beam Vapor Deposition for Large Resistive Switching Memristors

FEDERICO VITTORIO LUPO [1], MAURO MOSCA [1], SARUNAS BAGDZEVICIUS [2,3], RASHMI RANI [2], WILLIAM MAUDEZ [2], ESTELLE WAGNER [2], MARIA PIA CASALETTO [4], SALVATORE BASILE [1], GIACOMO BENVENUTI [5], ISODIANA CRUPI [1] (Senior Member, IEEE), AND ROBERTO MACALUSO [1] (Member, IEEE)

1 Thin Films Laboratory, Dipartimento di Ingegneria, Università degli Studi di Palermo, 90128 Palermo, Italy
2 3D-Oxides SAS, 01630 Saint-Genis-Poully, France
3 PIEMACS Sàrl, EPFL Innovation Parc, 1015 Lausanne, Switzerland
4 Institute of Nanostructured Materials, National Research Council, 90146 Palermo, Italy
5 ABCD Technology Sarl, 1260 Nyon, Switzerland

CORRESPONDING AUTHOR: R. MACALUSO (e-mail: roberto.macaluso@unipa.it)

This work was supported by the University of Palermo within the "*Premio Gruppi di Ricerca 2021*" of the Department of Engineering.

ABSTRACT We present chemical beam vapor deposition (CBVD) as a valuable technique for the fabrication of good quality HfO_2-based memristors. This deposition technique gives the opportunity to rapidly screen material properties in combinatorial mode and to reproduce the optimized conditions homogenously on large substrates. Cu/HfO_2/Pt memory devices with three different oxide thicknesses were fabricated and electrically characterized. A bipolar resistive switching and forming free behavior was seen in all the tested devices. Lower switching voltages than similar devices fabricated by employing different deposition techniques were observed. The conduction mechanism in the low resistance state can be ascribed to filamentary copper, while a trap-controlled space charge limited current conduction was observed in the high resistance state. The comparative evaluation of devices with different oxide thicknesses allows to infer that devices with thicker HfO_2 film (25 nm) are more performing in terms of R_{OFF}/R_{ON} ratio (10^6), and reproducible resistive switching over more than 100 cycles in both low and high resistance states. Thinner oxide devices (20 nm and 16 nm), despite similar long retention time (10^4 s), and lower SET/RESET voltages show instead a smaller memory window and a switching instability. These results, compared also with other reported in literature for similar memristive structures realized with other deposition techniques, show that CBVD can be considered as a promising technique for realizing HfO_2-based non-volatile memory devices with good performance.

INDEX TERMS Resistive switching, memristors, CBRAM, chemical beam vapor deposition, HfO_2.

I. INTRODUCTION

Memristors are believed to replace flash memories as non-volatile memories in the near future because of their simple Metal-Insulator-Metal (MIM) structure, low power consumption, fast switching operations, large scalability and great integrability with CMOS technology [1], [2], [3], [4]. Metal oxides such as HfO_2 [3], [5], [6], Ta_2O_5 [7], TiO_2 [8], [9], and ZnO [10], are typical employed memristive materials. HfO_2 has been largely studied, beside of the natural compatibility with CMOS technology, because of its excellent performance, such as very high scalability, low energy consumption per bit operation [11], [12], large bit per cell storage capability [13], and ultrafast switching [14]. Together with the oxide active material, also the employed contacts play an important role on both memristors performance and conduction mechanism. Typically, memristors which employ inert metal contacts such as Pt, are driven by the so-called valence change conduction mechanism (VCM), in

which the mobile species are positively charged oxygen vacancies, while memristors employing two different types of metal contacts, one inert and the other one active (e.g., Cu or Ag), exhibit the electrochemical metallization (ECM) conduction mechanism, in which the mobile species are metal ions and the conductive filament (CF) is composed of metal atoms [2], [3], [13]. These two types of memories have also different characteristics, with ECM devices (called also conductive-bridge random access memories (CBRAMs)) exhibiting a larger resistance window (i.e., the ratio between the resistance at the high resistance or OFF state (HRS), and the resistance at the low resistance or ON state (LRS)) [2], and VCM devices displaying larger speed and endurance [3]. Recent studies have proposed another kind of resistive switching memory device, called hybrid RRAM (HRRAM), which is characterized by conductive filaments composed of both metal ions and oxygen vacancies [15].

Several deposition techniques have been employed for fabricating HfO_2-based memristors, noticeably, atomic layer deposition (ALD) [6], [16], [17], metal-organic chemical vapor deposition (MOCVD) [18], [19], sputtering [20], [21], [22], pulsed lased deposition [23], electron beam [24], [25], molecular beam epitaxy (MBE) [26], and anodizing [27]. All these technologies have advantages and drawbacks in terms of material quality and adequate versatility to be integrated into a well-established fabrication process such as the CMOS technology.

Chemical Beam Vapor Deposition (CBVD) [28], also referred to as high-vacuum chemical vapor deposition (CVD), is a hybrid deposition technique between CVD and MBE. It is gaining interest for depositing high quality oxides such as HfO_2 [29], mixed Hf-Nb oxides [30], $LiNbO_3$ [31], Hf-doped $LiNbO_3$ [32], TiO_2 [33], and $BaTiO_3$ [34]. Sybilla CBVD equipment of ABCD Technology has many practical advantages over CVD and MBE to target device production, including scalability to mass production by homogenous deposition on large substrates (present standard is 450 mm wafers with $\pm$ 1% homogeneity), high control of growth rate (from few nm/h up to several μm/h), possibility to deposit 3D patterns by additive growth [35] and to irradiate locally the growing film during the deposition process to modify locally physico-chemical properties [36]. On top of that, its powerful combinatorial facility, offers the remarkable advantage to play with various effective parameters of the film such as dopants insertion, composition and thickness, on single substrate in one deposition [37]. Consequently, optimization of the films with respect to these parameters are perfectly accurate, since they grow simultaneously in the same conditions.

In this work, we present, for the first time, memristive devices fabricated with HfO_2 films grown by CBVD, which show a very good resistive switching behavior. By employing CBVD capability to deposit films with different thickness under combinatorial approach on the same substrate within the same deposition run, devices with three different HfO_2 thickness were fabricated and characterized.

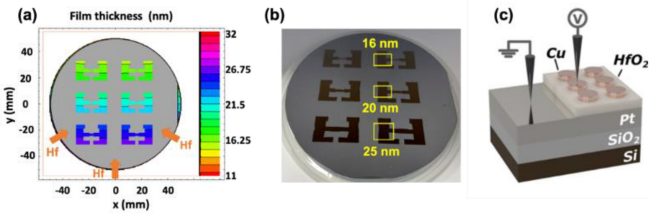

FIGURE 1. (a) Shadow mask (grey) and deposited film thickness estimation (color scale) in nm from deposition calibration. The three flow's directions from the three open Hf precursor sources are indicated with the orange arrows. (b) Photograph of the deposited HfO_2 film (brown areas) onto the Pt-coated SiO_2/Si wafer. The yellow squares highlight the selected regions that have been cleaved for obtaining the three samples with HfO_2 thickness of 16 nm, 20 nm and 25 nm. (c) Final structure of the Cu/HfO_2/Pt memristive devices with the electrical configuration employed for performing the electrical measurements.

II. EXPERIMENTAL

The fabrication process of the devices started with the sputtering of 100 nm-thick Pt bottom electrode onto a 4-inch SiO_2/Si substrate. Afterwards, a HfO_2 film with graded thickness from 16 nm to 25 nm along the Pt-coated SiO_2/Si wafer was deposited by CBVD [29], [37] through a shadow mask to leave portions of the Pt layer available to be contacted for the subsequent electrical characterization (see Fig. 1). The CBVD process employed a Hf precursor (Hf(mmp)4, CAS 309915 48 8, from Sigma Aldrich) which was evaporated from a thermostated reservoir (80.5 °C) without any carrier gas into the prechamber (14.8×10^{-3} mbar) from which it effuses towards the radiatively heated substrate (460 °C) in a combinatorial configuration (i.e., achieving a continuous thickness gradient as described in [30], [31], [32], [33], [34], [35], [37]) from three sources, through the shadow mask (see Fig. 1). HfO_2 deposition lasted 4275 s. Three different areas of the deposited HfO_2 film were subsequently cleaved in pieces of 2 cm $\times$ 2 cm (see Fig. 1(b)), cleaned with acetone and isopropanol, dried up with nitrogen, and employed for devices fabrication. Oxide thickness of the three samples, estimated from previous deposition calibration by reflectometry, was 16 nm, 20 nm, and 25 nm, respectively.

The memristor device structure was finished by depositing the Cu top electrode by thermal evaporation through a shadow mask consisting of 1 mm diameter circles (Fig. 1(c)).

HfO_2 films' structure and morphology was assessed by X-ray diffraction (Rigaku SmartLab, equipped with a Cu rotating anode, Kα radiation) and scanning electron microscopy (JEOL JEM-2100), respectively. Films surface composition was assessed by X-ray photoelectron spectroscopy through a VG Microtech ESCA3000 Multilab spectrometer equipped with a dual Al/Mg anode as X-Ray source, a five channeltrons detection system and a hemispheric analyser [38]. All devices were electrically characterized by means of a custom developed measurement system [39] which allows to perform both DC and AC pulse measurements.

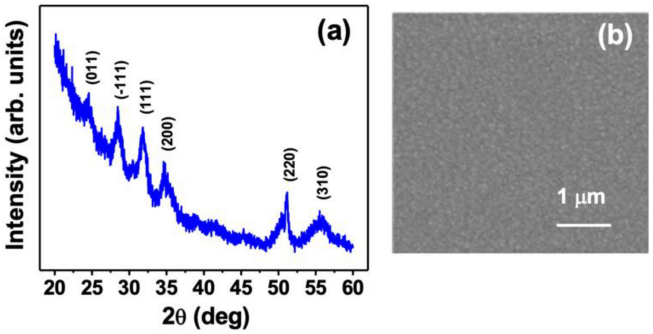

FIGURE 2. (a) XRD pattern of a 30 nm-thick HfO_2 film, and (b) SEM top view of the thickest HfO_2 film used for the fabrication of the memristive devices.

III. RESULTS AND DISCUSSION

A. STRUCTURAL AND MORPHOLOGICAL CHARACTERIZATION

Fig. 2(a) shows the X-ray diffraction (XRD) pattern, recorded in θ-2θ configuration, of a 30 nm-thick HfO_2 reference sample grown on Si substrate at 460 °C. All diffraction peaks can be assigned to the monoclinic phase of HfO_2 (ICDD 00-034-0104 card). A typical top view scanning electron microscope (SEM) image of the HfO_2 film grown onto the Pt/SiO_2/Si substrate is instead reported in Fig. 2(b). The film's surface looks compact and homogeneous, rough with small grains, and without any pinhole.

B. SURFACE CHEMICAL COMPOSITION CHARACTERIZATION

X-Ray Photoemission Spectroscopy (XPS) was used to investigate the deposition of the three HfO_2 films with different thickness and to determine their relative surface chemical composition. All the XPS measurements were performed without any additional pre-treatment of the samples. The binding energy (BE) scale was charge-corrected by using the C 1s peak (BE = 285.1 eV) due to the adventitious carbon on the surface. The accuracy of the BE measurement was ± 0.1 eV, whilst the relative atomic quantitative analysis had a ± 10% uncertainty. Photoelectron signals and peak components were assigned according to XPS literature reference database [40].

Hf 4f spectra of the three HfO_2 films with different thickness are reported in Fig. 3. The presence of a doublet peak with the Hf $4f_{7/2}$ component located at ~ BE = 17.3 eV and the Hf $4f_{5/2}$ component energy split by ΔE =1.65 eV corresponds to the presence of the Hf^{4+} species in the HfO_2 surface of 20 nm and 25 nm-thick films [41], [42], [43]. The curve-fitting of the O 1s spectra is reported in Fig. 4(a) for the bare Pt/SiO_2/Si substrate and in Fig. 4(b)-(d) for the HfO_2 films of 16, 20 and 25 nm thickness, respectively. The curve-fitting results are summarized in Table 1. The single component of the O 1s peak of the substrate shown in Fig. 4(a) is located at BE = 532.6 eV and assigned to SiO_2 [40]. This component, beside a small shift, is also present in the O 1s spectra of all HfO_2 films, regardless the thickness, as shown in Fig. 4(b)-(d) (blue dashed line). The

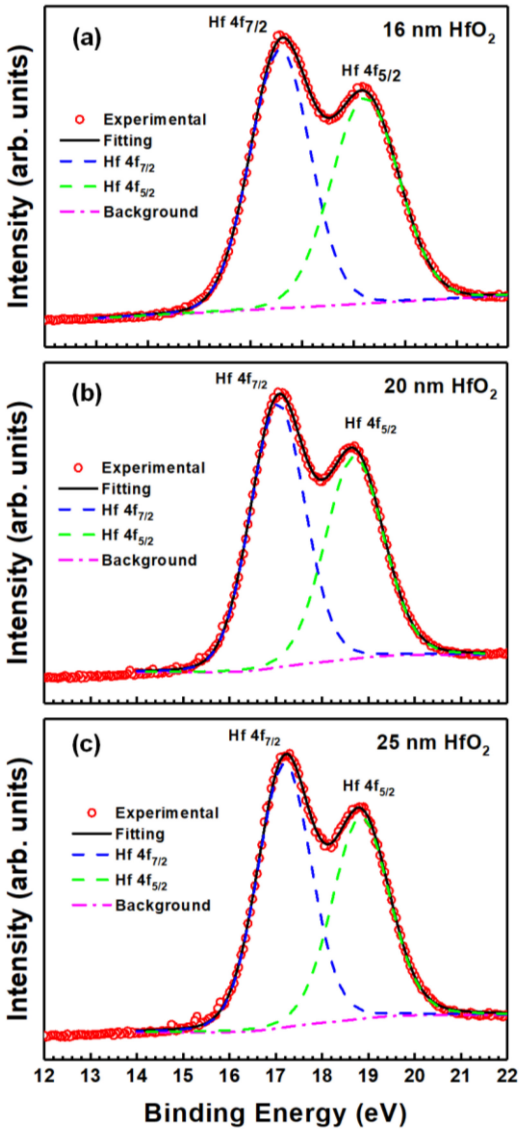

FIGURE 3. XPS curve-fitting of Hf 4f spectra of (a) 16 nm, (b) 20 nm, and (c) 25 nm thick HfO_2 films.

second component of the O 1s spectra of HfO_2 films, located at BE = 530.6 eV (green dashed line), corresponds to the presence of oxides and defective oxides species [40], [41].

The evidence that all hafnium oxide films are sub-stochiometric is also confirmed by the relative chemical composition of the surface listed in Table 2. Hf 4f and O 1s photoelectron signals can, in fact, be used in combination to determine the stoichiometry of the HfO_2 films. For the determination of the *O/Hf* atomic ratio, the contribution of the SiO_2 component deriving from the substrate and resulting from the curve-fitting of the O 1s peak, can be neglected in the calculation. Results are reported in Table 2 for the detected *O/Hf* and the calculated *O*/Hf* ratio. The surface relative chemical composition determined by XPS confirmed that all HfO_2 films are sub-stoichiometric with small differences between the values of the *O*/Hf* ratios. This result shows that CBVD is a valuable tool for the

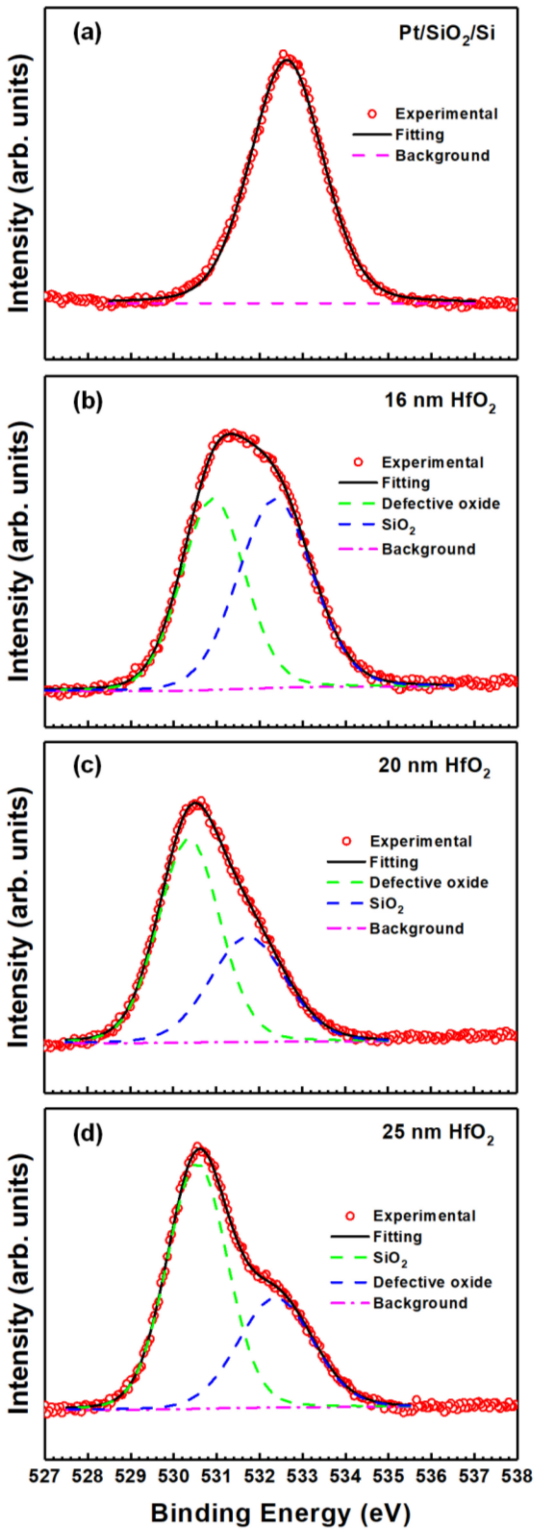

FIGURE 4. XPS curve-fitting of O 1s spectra of (a) bare $Pt/SiO_2/Si$ substrate, (b) 16 nm, (c) 20 nm and (d) 25 nm-thick HfO_2 films.

growth of chemically uniform HfO_2 films for the realization of memristive devices with different thickness on the same wafer.

TABLE 1. XPS results of Hf 4f and O 1s curve fitting in the investigated samples. The two spin-orbit Hf $4f_{7/2}$ and Hf $4f_{5/2}$ components of Hf 4f signal resulted energy split by $\Delta E = 1.65$ eV.

Sample	XPS signal	Binding energy [eV]	Peak assignment	Peak area [%]
Substrate	O 1s	532.6	SiO_2	100
16 nm HfO_2	Hf $4f_{7/2}$	17.5	HfO_2	100
16 nm HfO_2	O 1s	530.9	Oxides	36.4
16 nm HfO_2	O 1s	532.4	SiO_2	63.6
20 nm HfO_2	Hf $4f_{7/2}$	17.1	HfO_2	100
20 nm HfO_2	O 1s	530.4	Oxides	39.4
20 nm HfO_2	O 1s	531.8	SiO_2	60.6
25 nm HfO_2	Hf $4f_{7/2}$	17.2	HfO_2	100
25 nm HfO_2	O 1s	530.5	Oxides	35.8
25 nm HfO_2	O 1s	532.4	SiO_2	64.2

TABLE 2. XPS surface chemical composition of the investigated samples. Elemental concentration is expressed as atomic percentage (atom. %). The O*/Hf ratio was calculated after removing the contribution of the SiO_2 component (deriving from the substrate) from the O 1s peak (blue component in Fig. 4).

Sample	Hf 4f	O 1s	Si 2s	Pt 4f	*O/Hf*	*O*/Hf*
Substrate		25.3	54.2	20.5		
16 nm HfO_2	19.2	33.4	34.5	12.2	1.74	0.63
20 nm HfO_2	24.7	40.7	22.2	10.0	1.65	0.65
25 nm HfO_2	29.7	46.4	19.1	4.7	1.56	0.56

XPS data analysis highlights that, as expected, the concentration of the elements constituting the substrate (i.e., silicon and platinum), decreases as the HfO_2 films thickness increases. Moreover, by increasing the thickness of the HfO_2 films (from 16 nm to 25 nm), the surface amount of Hafnium and Oxygen increases.

C. ELECTRICAL CHARACTERIZATION OF THE DEVICES

The typical I-V characteristics of the three devices with different HfO_2 thickness are reported in Fig. 5. The voltage sweep was tailored to the different oxide thicknesses to avoid breakdown of the thinner oxide and both V_{SET} and V_{RESET} were below 1.4 V. All measured devices did not need a forming process and exhibited an anticlockwise hysteresis cycle as expected for memristors and a bipolar switching behavior, with the switching to the ON (or SET) state for positive voltages and the switching to the OFF (or RESET) state for negative voltages. Moreover, the memory window between R_{OFF} (>1 MΩ) and R_{ON} (≤ 100 Ω) exhibited by the thickest oxide devices was larger than 10^6.

Because of the $Cu/HfO_2/Pt$ structure, the conduction mechanism of the devices may be attributed, as well as many similar devices reported in literature [2], [16], [17], [22], [23], [44], [45] to the formation of Cu conductive filaments during the SET process and their subsequent rupture after having inverted the applied voltage (RESET process). This is confirmed by the ohmic behavior of the I-V characteristic during the ON state, as shown in the log-log plot reported in

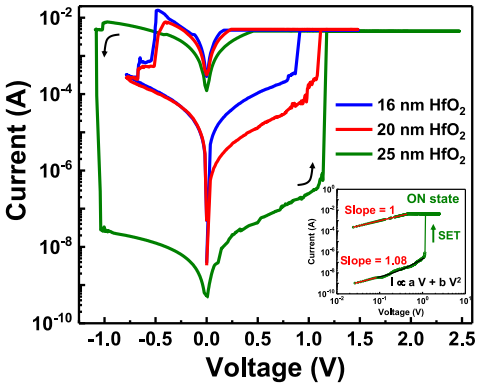

FIGURE 5. **Typical bipolar I-V resistive switching characteristics of the Cu/HfO_2/Pt memristors with different oxide thickness. The arrows indicate the direction of the hysteresis cycles. A current compliance of 5 mA was imposed during the SET process. The inset shows the I–V curve related to the 25 nm-thick oxide device replotted in a double logarithmic scale.**

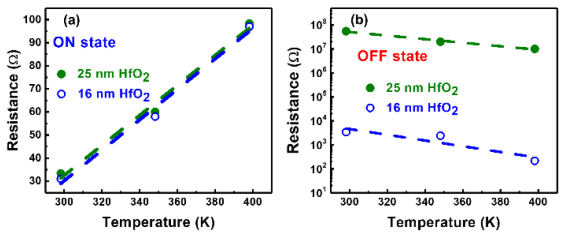

FIGURE 6. **Temperature dependence of R_{ON} (a) and R_{OFF} (b) relative to 16 nm and 25 nm-thick HfO_2 devices at the reading voltage of 0.1 V. The dashed lines are linear fitting.**

the inset of Fig. 5 [44], [46], and by the linear increase of R_{ON} with the temperature, as shown in Fig. 6(a) [24]. From the straight-line slope of Fig. 6(a) is possible, moreover, to estimate a temperature coefficient of 4×10^{-3} K^{-1}, in line with the value reported for high purity copper (3.9×10^{-3} K^{-1}) [47]. This suggests that the conducting filament is mainly composed by copper. The inset of Fig. 5 shows, furthermore, that the conduction mechanism in the HRS is characterized by a trap-controlled space charge limited current conduction (TC-SCLC) with a predominant ohmic behavior at low voltages and a more distinct quadratic behavior at higher voltages ($I \propto aV + bV^2$) [48]. This non-ohmic behavior of the HRS state is further evidenced by the variation of R_{OFF} with the temperature reported in Fig. 6(b), which corresponds to a typical semiconducting behavior, considering the approximate linear relationship between $\log(R_{OFF})$ and the temperature [24], [49], [50]. This variation, observed also in the 16 nm-thick oxide device, could be due to a large number of oxygen vacancy-related traps formed inside the HfO_2 film following the increase in temperature, with consequent increase of the injected current through the oxide [51], [52], [53]. From Fig. 5 is possible to see that V_{SET} increases with the oxide thickness, from 0.9 V to 1.1 V to 1.2 V, for 16 nm, 20 nm, and 25 nm thick HfO_2 films, respectively. This behavior has already been reported for Cu/HfO_2/Pt devices fabricated by ALD [17], and sputtering [22], and for other CBRAM devices [21], and means that a larger electric field is required in the thicker oxide devices to achieve the formation of Cu filaments [22]. On the other hand, the thickest oxide memristor exhibits also the largest V_{RESET} (−1.1 V) as it has been observed in [17] and [22], and also with other materials [54]. Both V_{SET} and V_{RESET} are however lower than those reported for devices with same structure and similar oxide thickness deposited by sputtering [22] and PLD [23] and devices which employ thinner HfO_2 films grown by ALD [16], [17], as it is possible to compare in Table 3. This finding is very promising for realizing low voltage memory devices.

Pulse measurements were performed to assess both data retention and endurance performance. Retention measurements of the three devices are reported in Figs. 7(a) and (b). As it can be seen, both R_{OFF} and R_{ON} of devices which employ thicker HfO_2 film (20 nm and 25 nm) are very stable within the testing period of 10^4 s. The larger oxide thickness makes R_{OFF} of the device with 25 nm-thick oxide larger than that of devices with 16 and 20 nm-thick oxide of 4 and 3 orders of magnitude, respectively. This very large difference could also be ascribed to larger leakage currents in thinner oxides [31], enhanced by the sub-stoichiometry of the films. On the other hand, R_{ON} is of the same order of magnitude for all devices, with the thinnest oxide device exhibiting a small variability over time (from 40 Ω to 7 Ω), which, however, does not compromise the integrity of the memory device, being the R_{OFF}/R_{ON} ratio always larger than 10, as shown in Fig. 7(b). The latter highlights also how the device with 25 nm-thick HfO_2 film exhibits the best R_{OFF}/R_{ON} ratio ($\sim 10^6$), which is much larger than similar devices realized by electron beam [26], PLD [23], and ALD [17]. This means that a proper deposited HfO_2 film thickness allows realizing memristive devices with a reliable non-volatile memory behavior [21].

Endurance measurements were carried out by continuously switching the devices from the OFF to the ON state and from the ON to the OFF state by applying positive and negative 0.5s-wide pulses, respectively. The measurements reported in Fig. 7(c), relative to the thickest oxide-based device, revealed that, although the fluctuations showed by R_{ON}, the switching between the ON and the OFF state in the first 117 switching cycles is adequately uniform ($R_{OFF}/R_{ON} \sim 10^6$), controllable, reversible, and reproducible [1], [55], [56], [57]. However, after 117 cycles, a progressive degradation (manifested as a reduction of resistance) of R_{OFF}, until the device gets stuck in the LRS, is observable. This behavior, which denotes a lower endurance than other works [58], [59], has been widely reported for ECM devices and could be ascribed to cycle to cycle irreversible penetration of copper atoms into the oxide layer which makes the switching layer progressively thinner and thinner [60], [61], [62], [63]. The variability of R_{ON} could be due to a different number and diameter of the conducting filaments formed during the SET process from cycle to cycle. Thinner oxides, instead, as it is shown in Figs. 7(d) and 7(e), give rise to unstable and unreliable devices which quite often fail to switch either to the ON or

TABLE 3. Comparison between the characteristics of the devices presented in this work and those of similar Cu/HfO_2/Pt memristive devices fabricated with different techniques. NA stands for not available.

Technique	Structure	t_{ox} [nm]	Vset/Vreset	Forming	R_{OFF}/R_{ON}	Retention [s]	Endurance [# cycles]	Ref.
CBVD	Cu/HfO_2/Pt	16	0.9 V/-0.5 V		6×10^1			
CBVD	Cu/HfO_2/Pt	20	1.1 V/-0.5 V	No	5×10^2	10^4	117	[This work]
CBVD	Cu/HfO_2/Pt	25	1.2V/-1.1V		10^6			
ALD	Cu/HfO_2/Pt	10	3 V/-2.3 V	No	NA	NA	NA	[16]
ALD	Cu/HfO_2/Pt	3	0.5 V/-0.5 V					
ALD	Cu/HfO_2/Pt	5	1.5 V/-0.6V	Yes	$< 10^4$	10^4	120	[17]
ALD	Cu/HfO_2/Pt	10	2.1 V/-0.8 V					
ALD	Cu/HfO_2/Pt	5	1.8 V/-0.8 V	Yes	$> 10^4$	10^4	10^7	[58, 59]
Sputtering	Cu/HfO_2/Pt	10	0.22 V/-0.12 V	No	NA	NA	NA	[20]
Sputtering	Cu/HfO_2/Pt	5	1 V/-1.4 V					
Sputtering	Cu/HfO_2/Pt	10	0.7 V/-0.7 V	Yes	NA	NA	NA	[22]
Sputtering	Cu/HfO_2/Pt	20	1.4 V-1 V					
Sputtering	Cu/HfO_2/Pt	30	3.5 V/-3.8 V					
PLD	Cu/HfO_2/Pt	30	2 V/-1.8 V	No	10^4	NA	80	[23]
Electron-beam	Cu/HfO_2/Pt	20	0.2 V/-0.2 V	No	10^2	NA	120	[19]
Electron-beam	Cu/*Cu:*HfO_2/Pt	40	4 V/-1.8V	No	10^7	10^5	100	[18]

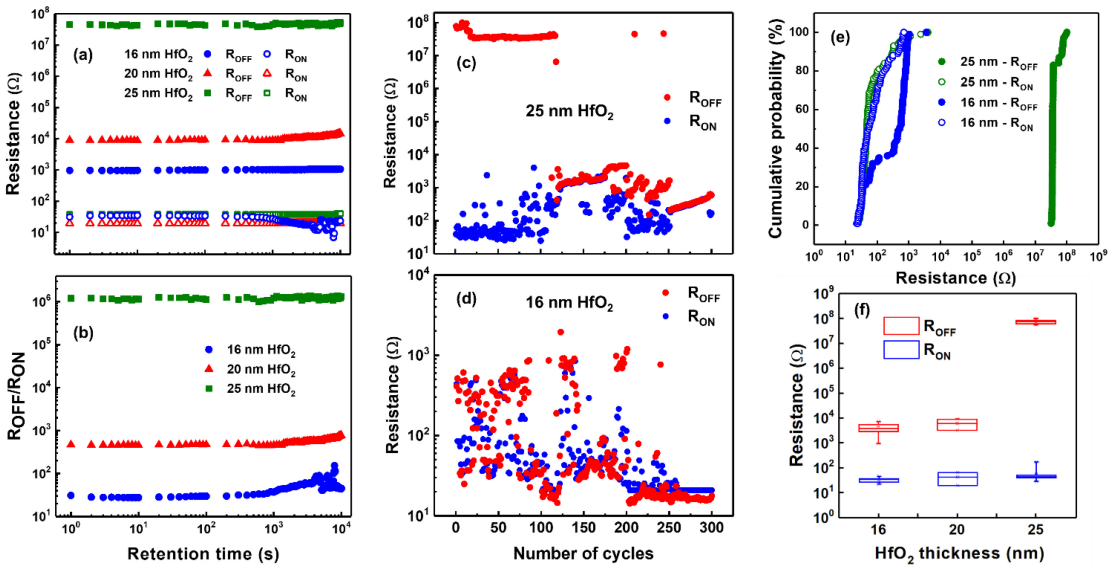

FIGURE 7. Retention characteristics of the Cu/HfO_2/Pt devices with different oxide thicknesses in terms of (a) R_{OFF} and R_{ON} and (b) R_{OFF}/R_{ON} ratio. All the retention measurements were performed by using a + 1.5 V, 0.5 s SET pulse followed by + 0.1 V, 0.5 s reading pulses for R_{ON} and a −1.5 V, 0.5 s RESET pulse followed by − 0.1 V, 0.5 s reading pulses for R_{OFF}. Endurance performance of (c) the thickest and (d) the thinnest oxide devices over 300 cycles of SET/RESET 0.5 s-wide pulses. All the reading measurements were performed at + 0.1 V (R_{ON}) and − 0.1 V (R_{OFF}). Cycle to cycle (100 cycles) cumulative probability of R_{ON} and R_{OFF} for the 16 nm and 25 nm-thick oxide devices (e). Device to device R_{ON} and R_{OFF} variability determined by measuring 20 different devices with the same oxide thickness for all three types of devices (f).

the OFF state and eventually remain in the LRS earlier than the thickest oxide device.

Cycle to cycle and device to device variations of R_{ON} and R_{OFF} for devices with different oxide thickness are reported in Figs. 7(e) and 7(f), respectively. Intra-device probability distributions of R_{ON} and R_{OFF} relative to the thickest oxide device show a good stability of R_{OFF} and a more variability of R_{ON}, which however does not invalidate the very good R_{OFF}/R_{ON} switching stability. The thinnest oxide device displays instead a larger cycle to cycle variability, due to the instability earlier described. Device to device uniformity statistical analysis (Fig. 7(f)), based on 20 devices of each type (16 nm, 20 nm and 25 nm oxide thickness), shows a superiority of the thickest oxide devices in terms of tightest distribution within R_{ON} and R_{OFF}, which implies a much greater reproducibility of results respect to the thinner devices.

IV. CONCLUSION

In summary, bipolar and forming-free memristors based on HfO_2 films deposited by CBVD were fabricated and characterized. SEM measurements showed that HfO_2 films

are uniform and crack-free. XPS measurements highlighted that all the deposited HfO_2 films are sub-stoichiometric. A comparative study was carried out to test the devices behavior against oxide thickness. Very good performance in terms of R_{OFF}/R_{ON} ratio ($\sim 10^6$ and $\sim 10^5$ at 298 K and 398 K, respectively), low switching voltages, and retention time over 10^4 s were shown by the devices with the thickest oxide film (25 nm), which however displayed a relatively low, albeit stable endurance of 117 cycles. Thinner oxide devices showed instead a reduced R_{OFF}/R_{ON} ratio ($\sim$ 500 and $\sim$ 60 for 20 nm and 16 nm HfO_2 films, respectively), a still good retention, and a more and more degrading endurance and uniformity with decreasing oxide thickness. Data analysis allowed us to explain the switching mechanism, which can be ascribed to the formation and rupture of copper filaments. In the LRS the conduction mechanism was ohmic, while the HRS is characterized by the TC-SCLC mechanism. The observed filamentary effect suggests that the active medium is actually much smaller than the cell size, providing a potential of scaling [49]. A comparison with other similar devices realized with different deposition techniques showed that CBVD-grown HfO_2 films of appropriate thickness provide memory devices with lower SET and RESET voltages, larger resistance window and retention, and lower endurance. This means that CBVD can thus be considered as a promising deposition technique for the fabrication of large resistive switching HfO_2-based non-volatile memory devices.

ACKNOWLEDGMENT

The authors would like to thank Dr. G. Nasillo of ATeN Center (University of Palermo) for the SEM characterization.

REFERENCES

[1] H.-S. P. Wong et al., "Metal-oxide RRAM," *Proc. IEEE*, vol. 100, no. 6, pp. 1951–1971, Jun. 2012, doi: 10.1109/JPROC.2012.2190369.

[2] D. Ielmini, "Resistive switching memories based on metal oxides: Mechanisms, reliability and scaling," *Semicond. Sci. Technol.*, vol. 31, May 2016, Art. no. 63002, doi: 10.1088/0268-1242/31/6/063002.

[3] F. Zahoor, T. Z. A. Zulkifl, and F. A. Khanday, "Resistive random access memory (RRAM): An overview of materials, switching mechanism, performance, multilevel cell (MLC) storage, modeling, and applications," *Nanoscale Res. Lett.*, vol. 15, p. 90, Apr. 2020, doi: 10.1186/s11671-020-03299-9.

[4] W. Banerjee, "Challenges and applications of emerging non-volatile memory devices," *Electronics*, vol. 9, p. 1029, Jun. 2020, doi: 10.3390/electronics9061029.

[5] A. S. Sokolov et al., "Influence of oxygen vacancies in ALD HfO_{2-x} thin films on non-volatile resistive switching phenomena with a Ti/HfO_{2-x}/Pt structure," *Appl. Surface Sci.*, vol. 434, pp. 822–830, Mar. 2018, doi: 10.1016/j.apsusc.2017.11.016.

[6] Z. Zhang, Y. Wu, H.-P. Wong, and S. S. Wong, "Nanometer-scale HfO_x RRAM," *IEEE Electron Device Lett.*, vol. 34, no. 8, pp. 1005–1007, Aug. 2013, doi: 10.1109/LED.2013.2265404.

[7] A. Prakash, D. Jana, and S. Maikap, "TaO_x-based resistive switching memories: prospective and challenges," *Nanoscale Res. Lett.*, vol. 8, p. 418, Oct. 2013, doi: 10.1186/1556-276X-8-418.

[8] V. Aglieri et al., "Resistive switching in microscale anodic titanium dioxide-based memristors," *Superlattices Microstruct.*, vol. 113, pp. 135–142, Jan. 2018, doi: 10.1016/j.spmi.2017.10.031.

[9] V. Aglieri et al., "Forming-free and self-rectifying resistive switching effect in anodic titanium dioxide-based memristors," in *Proc. IEEE 4th Int. Forum Res. Technol. Soc. Ind. (RTSI)*, 2018, pp. 1–4, doi: 10.1109/RTSI.2018.8548396.

[10] R. Macaluso et al., "Resistive switching behaviour in ZnO and VO_2 memristors grown by pulsed laser deposition," *Electron. Lett.*, vol. 50, no. 4, pp. 262–263, Feb. 2014, doi: 10.1049/el.2013.3175.

[11] B. Govoreanu et al., "Performance and reliability of ultra-thin HfO_2-based RRAM (UTO-RRAM)," in *Proc. 5th IEEE Int. Memory Workshop*, 2013, pp. 48–51, doi: 10.1109/IMW.2013.6582095.

[12] B. Govoreanu et al., "$10\times10nm^2$ Hf/HfO_x crossbar resistive RAM with excellent performance, reliability and low-energy operation," in *Proc. Int. Electron Devices Meeting*, Washington, DC, USA, 2011, pp. 31.6.1–31.6.4, doi: 10.1109/IEDM.2011.6131652.

[13] W. Banerjee, S. Hun Kim, S. Lee, D. Lee, and H. Hwang, "An efficient approach based on tuned nanoionics to maximize memory characteristics in Ag-based devices," *Adv. Electron. Mater.*, vol. 7, Mar. 2021, Art. no. 2100022, doi: 10.1002/aelm.202100022.

[14] C. Wanf et al., "Ultrafst reset analysis of HfO_x based RRAM by subnanosecond pulses," *Adv. Electron. Mater*, vol. 3, Oct. 2017, Art. no. 1700263, doi: 10.1002/aelm.201700263.

[15] G. Sassin et al., "Hybrid-RRAM toward next generation of nonvolatile memory: Coupling of oxygen vacancies and metal ions," *Adv. Electron. Mater.*, vol. 5, Jan. 2019, Art. no. 1800658, doi: 10.1002/aelm.201800658.

[16] M. Saadi et al., "On the mechanisms of cation injection in conducting bridge memories: The case of HfO_2 in contact with noble metal anodes (Au, Cu, Ag)," *J. Appl. Phys.*, vol. 119, 2019, Art. no. 114501, doi: 10.1063/1.4943776.

[17] M. Wang et al., "Investigation of one-dimensional thickness scaling on $Cu/HfO_x/Pt$ resistive switching device performance," *IEEE Electron Device Lett.*, vol. 33, no. 11, pp. 1556–1558, Nov. 2012, doi: 10.1109/LED.2012.2211563.

[18] H.-D. Kim, M. J. Yun, and S. Kim, "Resistive switching phenomena of HfO_2 films grown by MOCVD for resistive switching memory devices," *J. Korean Phys. Soc.*, vol. 69, no. 3, pp. 439–442, Aug. 2016, doi: 10.3938/jkps.69.439.

[19] S. Lee, W. G. Kim, S. W. Rhee, and K. Yong, "Resistance switching behaviors of hafnium oxide films grown by MOCVD for nonvolatile memory applications," *J. Electrochem. Soc.*, vol. 155, no. 2, pp. H92–H96, 2008, doi: 10.1149/1.2814153.

[20] M. Zhang et al., "Analysis on the filament structure evolution in reset transition of Cu/HfO_2/Pt RRAM device," *Nanoscale Res. Lett.*, vol. 11, p. 269, May 2016, doi: 10.1186/s11671-016-1484-8.

[21] D. Ito, Y. Hamada, S. Otsuka, T. Shimizu, and S. Shingubara, "Oxide thickness dependence of resistive switching characteristics for Ni/HfO_x/Pt resistive random access memory device," *Jpn. J. Appl. Phys.*, vol. 54, Jun. 2015, Art. no. 6FH11, doi: 10.7567/JJAP.54.06FH11.

[22] S. Chen and I. Valov, "Design of materials configuration for optimizing redox-based resistive switching memories," *Adv. Mater.*, vol. 34, no. 3, Oct. 2021, Art. no. 2105022, doi: 10.1002/adma.202105022.

[23] T. Nagata, M. Haemori, Y. Yamashita, H. Yoshikawa, K. Kobayashi, and T. Chikyow, "Observation of filament formation process of Cu/HfO_2/Pt ReRAM structure by hard X-ray photoelectron spectroscopy under bias operation," *J. Mater. Res.*, vol. 27, no. 6, pp. 869–878, 2012, doi: 10.1557/jmr.2011.448.

[24] Y. Wang et al., "Investigation of resistive switching in Cu-doped HfO_2 thin film for multilevel non-volatile memory applications," *Nanotechnology*, vol. 21, no. 4, 2010, Art. no. 45202, doi: 10.1088/0957-4484/21/4/045202.

[25] W. Lian et al., "Improved resistive switching uniformity in Cu/HfO_2/Pt devices by using current sweeping mode," *IEEE Electron. Dev. Lett.*, vol. 32, no. 8, pp. 1053–1055, Aug. 2011, doi: 10.1109/LED.2011.2157990.

[26] P. Calka et al., "Engineering of the chemical reactivity of the Ti/HfO_2 interface for RRAM: Experiment and theory," *Appl. Mater. Interfaces*, vol. 6, no. 7, pp. 5056–5060, Mar. 2014, doi: 10.1021/am500137y.

[27] A. Zaffora, R. Macaluso, H. Habazaki, I. Valov, and M. Santamaria, "Electrochemically prepared oxides for resistive switching devices," *Electrochimica Acta*, vol. 274, pp. 103–111, Jun. 2018, doi: 10.1016/j.electacta.2018.04.087.

[28] E. Wagner, W. Maudez, S. Bagdzevicius, C. S. Sandu, and G. Benvenuti, "Chemical beam vapour deposition technique with Sybilla equipment: Review of main results in its 20-year anniversary," in *Proc. 12th SPIE Oxide-Based Mater. Devices*, 2021, Art. no. 116871Z, doi: 10.1117/12.2591443.
[29] R. Rani et al., "CBVD grown HfO_2 on TiN for high-precision MIM capacitor," *Physica B, Condens. Matter*, vol. 650, Feb. 2023, Art. no. 414541, doi: 10.1016/j.physb.2022.414541.
[30] A. Dabirian et al., "Combinatorial discovery and optimization of amorphous HfO_2-Nb_2O_5 mixture with improved transparency," *Electrochem. Solid State Lett.*, vol. 13, no. 7, pp. G60–G63, Apr. 2010, doi: 10.1149/1.3407618.
[31] A. Dabirian et al., "Combinatorial chemical beam epitaxy of lithium niobate thin films on sapphire," *J. Electrochem. Soc.*, vol. 158, no. 2, pp. D72–D76, Dec. 2011, doi: 10.1149/1.3519843.
[32] A. Dabirian et al., "Combinatorial high-vacuum chemical vapor deposition of textured hafnium-doped lithium niobate thin films on sapphire," *Cryst. Growth Des.*, vol. 11, no. 1, pp. 203–209, 2010, doi: 10.1021/cg1011583.
[33] D. Bijou et al., "Study of titanium amino-alkoxide derivatives as TiO_2 chemical beam vapour deposition precursor," *Mater. Chem. Phys.*, vol. 277, Feb. 2022, Art. no. 125561, doi: 10.1016/j.matchemphys.2021.125561.
[34] M. Reinke, Y. Kuzminykh, and P. Hoffmann, "Combinatorial HV-CVD survey of barium triisopropyl cyclopentadienyl and titanium tetraisopropoxide for the deposition of BaTiO3," *Physica Status Solidi*, vol. 212, no. 7, pp. 1556–1562, 2015, doi: 10.1002/pssa.201532326.
[35] E. Wagner, C. S. Sandu, S. Harada, G. Benvenuti, V. Savu, and P. Muralt, "Fabrication of complex oxide microstructures by combinatorial chemical beam vapour deposition through stencil masks," *Thin Solid Films*, vol. 586, pp. 64–69, 2015, doi: 10.1016/j.tsf.2015.04.021.
[36] G. Benvenuti, C. S. Sandu, and E. Wagner, "TiO_2 laser and electron beam assisted chemical deposition," *IOP Conf. Seri., Mater. Sci. Eng.*, vol. 8, 2010, Art. no. 12006, doi: 10.1088/1757-899X/8/1/012006.
[37] E. Wagner et al., "Geometry of chemical beam vapor deposition system for efficient combinatorial investigations of thin oxide films: deposited film properties versus precursor flow simulations," *ACS Comb. Sci.*, vol. 18, no. 3, pp. 154–161, 2016, doi: 10.1021/acscombsci.5b00146.
[38] D. Scirè et al., "Density of states characterization of TiO_2 films deposited by pulsed laser deposition for heterojunction solar cells," *Nano Res.*, vol. 15, no. 5, pp. 4048–4057, 2022, doi: 10.1007/s12274-021-3985-8.
[39] F. V. Lupo, D. Scirè, M. Mosca, I. Crupi, L. Razzari, and R. Macaluso, "Custom measurement system for memristor characterisation," *Solid State Electronics*, vol. 186, 2021, Art. no. 108049, doi: 10.1016/j.sse.2021.108049.
[40] A. V. Naumkin, A. Kraut-Vass, S. W. Gaarenstroom, and C. J. Powell (Nat. Inst. Stand. Technol., Gaithersburg, MD, USA). *NIST X-ray Photoelectron Spectroscopy Database: NIST Standard Reference Database 20, Version 4.1*. 2000. Accessed: Jul. 1, 2021. [Online]. Available: https://srdata.nist.gov/xps/
[41] D. Barreca, A. Milanov, R. A. Fischer, A. Devi, and E. Tondello, "Hafnium oxide thin film grown by ALD: An XPS study," *Surf. Sci. Spectra*, vol. 14, pp. 34–40, Dec. 2007, doi: 10.1116/11.20080401.
[42] G. D. Wilk, R. M. Wallace, and J. M. Anthony, "Hafnium and zirconium silicates for advanced gate dielectrics," *J. Appl. Phys.*, vol. 87, pp. 484–492, Jan. 2000, doi: 10.1063/1.371888.
[43] H. Wang, P. Wu, X. F. Li, S. Chen, S. P. Zhang, and B. B. Song, "Study of reactions between HfO_2 and Si in thin films with precise identification of chemical states by XPS," *Appl. Surf. Sci.*, vol. 257, no. 8, pp. 3440–3445, 2011, doi: 10.1016/j.apsusc.2010.11.042.
[44] X. Yang et al., "Investigation on the RESET switching mechanism of bipolar Cu/HfO_2/Pt RRAM devices with a statistical methodology," *J. Phys. D, Appl. Phys.*, vol. 46, no. 24, 2013, Art. no. 245107, doi: 10.1088/0022-3727/46/24/245107.
[45] W.-M. Chung et al., "A study of the relationship between endurance and retention reliability for a HfO_x-based resistive switching memory," *IEEE Trans. Device Mater. Rel.*, vol. 20, no. 3, pp. 541–547, Sep. 2020, doi: 10.1109/TDMR.2020.3007172.
[46] S.-C. Tsai et al., "Structural analysis and performance in a dual-mechanism conductive filament memristor," *Adv. Electron. Mater.*, vol. 7, no. 10, 2021, Art. no. 2100605, doi: 10.1002/aelm.202100605.
[47] J. Rumble, *Handbook of Chemistry and Physics*. Boca Raton, FL, USA: CRC Press, 1993.
[48] A. Beck, J. G. Bednorz, C. Gerber, C. Rossel, and D. Widmer, "Reproducible switching effect in thin oxide films for memory applications," *Appl. Phys. Lett.* vol. 77, pp. 139–141, Jul. 2000, doi: 10.1063/1.126902.
[49] Y. C. Yang, F. Pan, Q. Liu, M. Liu, and F. Zeng, "Fully room-temperature-fabricated nonvolatile resistive memory for ultrafast and high-density memory application," *Nano Lett.*, vol. 9, no. 4, pp. 1636–1643, Feb. 2009, doi: 10.1021/nl900006g.
[50] T. Tan et al. "Charge transport and bipolar switching mechanism in a Cu/HfO_2 /Pt resistive switching cell," *Chin. Phys. B*, vol. 25, Sep. 2016, Art. no. 117306, doi: 10.1088/1674-1056/25/11/117306.
[51] C. Walczyk et al., "Impact of temperature on the resistive switching behavior of embedded HfO_2-based RRAM devices," *IEEE Trans. Electron Devices*, vol. 58, no. 9, pp. 3124–3131, Sep. 2011, doi: 10.1109/TED.2011.2160265.
[52] L. Vandelli, A. Padovani, L. Larcher, R. G. Southwick, W. B. Knowlton, and G. Bersuker, "A physical model of the temperature dependence of the current through SiO_2/HfO_2 stacks," *IEEE Trans. Electron Devices*, vol. 58, no. 9, pp. 2878–2887, Sep. 2011, doi: 10.1109/TED.2011.2158825.
[53] Z. Fang et al., "Temperature instability of resistive switching on HfO_x-based RRAM devices," *IEEE Electron Device Lett.*, vol. 31, no. 5, pp. 476–478, May 2010, doi: 10.1109/LED.2010.2041893.
[54] A. Bricalli, E. Ambrosi, M. Laudato, M. Maestro, R. Rodriguez, and D. Ielmini, "Resistive switching device technology based on silicon oxide for improved ON–OFF ratio—Part I: Memory devices," *IEEE Trans. Electron Devices*, vol. 65, no. 1, pp. 115–121, Jan. 2018, doi: 10.1109/TED.2017.2777986.
[55] F. Pan, S. Gao, C. Chen, C. Song, and F. Zeng, "Recent progress in resistive random access memories: Materials, switching mechanisms, and performance," *Mater. Sci. Eng. R, Rep.*, vol. 83, pp. 1–59, Sep. 2014, doi: 10.1016/j.mser.2014.06.002.
[56] A. Fantini et al., "Intrinsic switching variability in HfO_2 RRAM," in *Proc. 5th IEEE Int. Memory Workshop*, 2013, pp. 30–33, doi: 10.1109/IMW.2013.6582090.
[57] S. Ambrogio, S. Balatti, A. Cubeta, A. Calderoni, N. Ramaswamy, and D. Ielmini, "Statistical fluctuations in HfO_x resistive-switching memory: Part I—Set/reset variability," *IEEE Trans. Electron Devices*, vol. 61, no. 8, pp. 2912–2919, Aug. 2014, doi: 10.1109/TED.2014.2330200.
[58] W. Banerjee, A. Kashir, and S. Kamba, "Hafnium oxide (HfO_2)—A multifunctional oxide: A review on the prospect and challenges of hafnium oxide in resistive switching and ferroelectric memories," *Small*, vol. 18, no. 23, May 2022, Art. no. 2107575, doi: 10.1002/smll.202107575.
[59] X. Zhao et al., "Confining cation injection to enhance CBRAM performance by nanopore graphene layer," *Small*, vol. 13, no. 35, Feb. 2017, Art. no. 1603948, doi: 10.1002/smll.201603948.
[60] M. Arita, A. Takahashi, Y. Ohno, A. Nakane, A. Tsurumaki-Fukuchi, and Y. Takahashi, "Switching operation and degradation of resistive random access memory composed of tungsten oxide and copper investigated using *in-situ* TEM," *Sci. Rep.*, vol. 5, Nov. 2015, Art. no. 17103, doi: 10.1038/srep17103.
[61] S. Balatti et al., "'Voltage-controlled cycling endurance of HfO_x-based resistive-switching memory," *IEEE Trans. Electron Devices*, vol. 62, no. 10, pp. 3365–3372, Oct. 2015, doi: 10.1109/TED.2015.2463104.
[62] M. Arita, A. Tsurumaki-Fukuchi, and Y. Takahashi, "Filamentary switching of ReRAM investigated by in-situ TEM," *Jpn. J. Appl. Phys.*, vol. 59, Mar. 2020, Art. no. SG0803, doi: 10.35848/1347-4065/ab709d.
[63] Y. Yang et al., "Probing electrochemistry at the nanoscale: In situ TEM and STM characterizations of conducting filaments in memristive devices," *J. Electroceram.*, vol. 39, pp. 73–93, Feb. 2017, doi: 10.1007/s10832-017-0069-y.

Open Access funding provided by 'Università degli Studi di Palermo' within the CRUI CARE Agreement